MECANIQUE DES FLUIDES
FLUIDS MECHANICS

RECENT ADVANCES IN COMPUTATIONAL FLUID DYNAMICS*

T. D. Butler
University of California
Los Alamos Scientific Laboratory
Los Alamos, New Mexico 87544
U.S.A.

I. INTRODUCTION

The use of high speed computers has opened new frontiers for the analysis and understanding of the complex processes in multi-dimensional transient fluid dynamics. Phenomena, heretofore intractable by analytical approaches or either difficult or impossible to study by experimental means, can be investigated in detail by numerical approaches. One of the most common of the numerical approaches is to approximate the non-linear partial differential equations that govern the dynamics by finite difference equations and solve them algebraically using the computer.

A number of different techniques have been devised to solve these difference equations [see, for example Harlow (1970)]. The purpose of this paper is to briefly describe two of the more successful and widely used methods: (1) the Marker and Cell (MAC) Method for incompressible flows with free surfaces, and (2) the Implicit Continuous-fluid Eulerian (ICE) Method that applies to flows that range from supersonic to the far subsonic regimes. In addition, some recent refinements and extensions to the basic methods are reviewed. However, no attempt is made in this paper to present detailed descriptions of the methods or their extensions; this is left to the references cited in the text.

Because of their general applicability, these two methods have been used to study numerous complex flow problems. For example, the MAC method, discussed in Sec. II, has been applied to such diverse problems as free surface flows under sluice gates and behind broken dams, the two-fluid non-linear Rayleigh-Taylor instability problem, the von Karman vortex street, and the run up of waves upon a beach. More recently the technique has been applied to problems in three space dimensions for investigations such as the transport of pollutants around structures, the dynamics of intense atmospheric vortices, and free-surface flows around submerged and exposed obstacles.

In Sec. III, we discuss the ICE method. Because of its ability to calculate flows of arbitrary Mach number, it has been used to analyze the dynamics resulting from intense atmospheric explosions from the early time highly compressible flow

*This work was performed under the auspices of the United States Atomic Energy Commission.

phase to the late time buoyant rise of the fireball. In addition, it is being used to study (1) the dynamics of continuous wave chemical lasers including the mixing and chemical reactions between species and the accompanying heat release, and (2) the flow patterns that result when a tritium ion beam impinges on a jet target of deuterium producing neutrons and releasing heat energy in the deuterium jet.

II. THE MARKER AND CELL METHOD

The MAC computing method [Harlow and Welch (1965)] and its simplified version referred to as SMAC [Harlow and Amsden (1970)] are well established schemes that calculate incompressible flows with or without free surfaces. The methods derive their names from the Lagrangian marker particles that move through the fixed mesh of cells and represent the flow of fluid. These techniques are quite general in their applicability to incompressible flow problems and have been widely used to analyze a variety of flow problems.

Briefly, the MAC technique solves the Navier-Stokes equations subject to the constraint that the divergence of the velocity field must vanish in any local region of the fluid. This is accomplished in MAC for each computational cell in the mesh. The pressure field is determined as a consequence of this condition by solving a Poisson-like equation. SMAC is an improvement over the original MAC because of the ease of applying the fluid boundary conditions. Of particular concern in the MAC scheme is the method of handling the pressures in fictitious cells exterior to the computing region of interest. SMAC simplifies this handling by assuring a homogeneous boundary condition for the pressure at rigid walls.

In this section, a new iteration algorithm is described that offers further ease in applying the boundary conditions and eliminates the computation of pressures in fictitious cells altogether. Hirt and Cook (1972) used this algorithm in their application of the MAC method to problems in three space dimensions. In addition, an improved treatment of the free surface boundary condition is presented.

A. Solution Procedure

The governing equations of fluid motion for incompressible flows in two-dimensional Cartesian coordinates are

$$\frac{\partial u}{\partial x} + \frac{\partial v}{\partial y} = 0 \tag{1}$$

$$\frac{\partial u}{\partial t} + \frac{\partial u^2}{\partial x} + \frac{\partial uv}{\partial y} = -\frac{\partial \phi}{\partial x} + \frac{\partial \sigma_{xx}}{\partial x} + \frac{\partial \sigma_{xy}}{\partial y} \tag{2}$$

$$\frac{\partial v}{\partial t} + \frac{\partial uv}{\partial x} + \frac{\partial v^2}{\partial y} = -\frac{\partial \phi}{\partial y} + \frac{\partial \sigma_{xy}}{\partial x} + \frac{\partial \sigma_{yy}}{\partial y} \tag{3}$$

in which u and v are the velocity components in the x and y directions, respectively, and ϕ is the pressure divided by the constant density. The stress tensor terms are given by

$$\sigma_{xx} = 2\nu \frac{\partial u}{\partial x}$$

$$\sigma_{xy} = \nu \left(\frac{\partial u}{\partial y} + \frac{\partial v}{\partial x} \right) \tag{4}$$

$$\sigma_{yy} = 2\nu \frac{\partial v}{\partial y}$$

where ν is the kinematic viscosity. Equations (1) - (3) are written in conservative form for approximation by finite differences.

The grid layout, shown in Fig. 1, indicates the location of the various quantities within a computational cell. It is noted that the velocities are centered on the cell boundaries with the pressure a cell centered quantity. The diagonal components of the stress tensor are likewise cell centered values while the off-diagonal elements are computed at cell vertices. The i,j indices in this figure denote spatial position in the computing mesh.

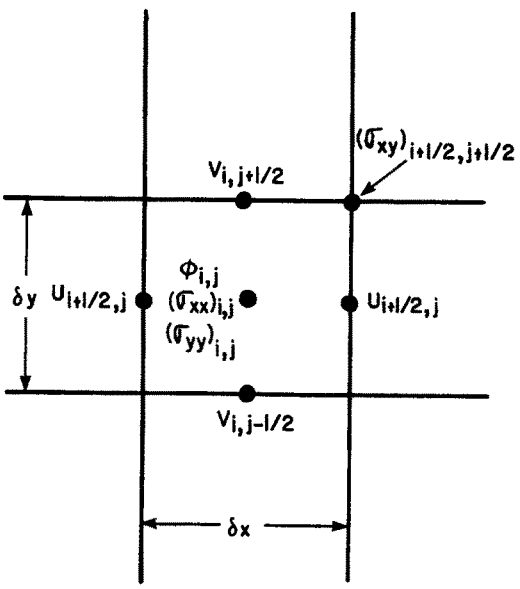

Figure 1

As a first step in the solution procedure, intermediate values of velocity, denoted by tildes, are computed for each cell. For the x-component of velocity, the tilde value on the right hand side of cell (i,j) is given by

$$\tilde{u}_{i+\frac{1}{2},j} = u^n_{i+\frac{1}{2},j} - \delta t \left\{ \frac{1}{\delta x} \left[(u^2)^n_{i+1,j} - (u^2)^n_{i,j} \right] + \frac{1}{\delta y} \left[(uv)^n_{i+\frac{1}{2},j+\frac{1}{2}} - (uv)^n_{i+\frac{1}{2},j-\frac{1}{2}} \right] \right.$$

$$+ \frac{1}{\delta x} \left[\phi^n_{i+1,j} - \phi^n_{i,j} \right] + \frac{1}{\delta x} \left[(\sigma_{xx})^n_{i,j} - (\sigma_{xx})^n_{i+1,j} \right]$$

$$\left. + \frac{1}{\delta y} \left[(\sigma_{xy})^n_{i+\frac{1}{2},j-\frac{1}{2}} - (\sigma_{xy})^n_{i+\frac{1}{2},j+\frac{1}{2}} \right] \right\} \tag{5}$$

in which δt is the time step and the time levels are indicated by the superscripts. Straightforward averages and centered differences may be used in each term.

An analogous formula is derived for the $\tilde{v}_{i,j+\frac{1}{2}}$. It should be noted, however, that no intermediate values are computed for velocities located on inflow boundaries, rigid boundaries, or velocities exterior to the computing region of interest. Thus, a normal velocity component on a rigid wall remains zero, and the velocity at an inflow boundary is unchanged from its prescribed value.

After computing the appropriate tilde components of velocity, the finite difference analogy to Eqn. (1) is not satisfied in general for every cell in the mesh. This necessitates computing modifications to the pressures and velocities using an iteration algorithm.

The desire is to find a velocity field consistent with the boundary conditions such that

$$D^{n+1}_{i,j} = 0 \tag{6}$$

where

$$D_{i,j} = \frac{1}{\delta x} \left(u_{i+\frac{1}{2},j} - u_{i-\frac{1}{2},j} \right) + \frac{1}{\delta y} \left(v_{i,j+\frac{1}{2}} - v_{i,j-\frac{1}{2}} \right) , \tag{7}$$

and the superscript in Eqn. (6) refers to the new time level n+1 for the velocity values. In practice, an iteration procedure is used, which changes the cell pressures and velocities until Eqn. (6) is satisfied within acceptable limits.

To initiate the iteration, the tilde velocities for cell (i,j) are inserted into Eqn. (7). If $D_{i,j} > 0$ as a result, there has been a mass loss in the cell; if $D_{i,j} < 0$, a mass gain. To correct the values, the pressure is changed by an amount $\delta\phi_{i,j}$ obtained from the expansion

$$D^{n+1}_{i,j} - D_{i,j} = \left(\frac{\partial D}{\partial \phi} \right)_{i,j} \delta\phi_{i,j}$$

and the requirement of Eqn. (6). Thus, we have

$$\delta\phi_{i,j} = -\frac{\omega D_{i,j}}{\left(\frac{\partial D}{\partial \phi}\right)_{i,j}} \tag{8}$$

where ω is an over-relaxation factor that has the range $1 \leq \omega \leq 2$. The denominator in Eqn. (8) is constant for every cell and is given by

$$\left(\frac{\partial D}{\partial \phi}\right)_{i,j} = 2\delta t \left[\frac{1}{\delta x^2} + \frac{1}{\delta y^2}\right] \tag{9}$$

Once $\delta\phi_{i,j}$ is determined, the quantities are updated:

$$\begin{aligned}
{}^{h+1}\phi_{i,j} &= {}^{h}\phi_{i,j} + \delta\phi_{i,j} \\
{}^{h+1}u_{i+\frac{1}{2},j} &= {}^{h}u_{i+\frac{1}{2},j} + \frac{\delta t}{\delta x}\,\delta\phi_{i,j} \\
{}^{h+1}u_{i-\frac{1}{2},j} &= {}^{h}u_{i-\frac{1}{2},j} - \frac{\delta t}{\delta x}\,\delta\phi_{i,j} \\
{}^{h+1}v_{i,j+\frac{1}{2}} &= {}^{h}v_{i,j+\frac{1}{2}} + \frac{\delta t}{\delta y}\,\delta\phi_{i,j} \\
{}^{h+1}v_{i,j-\frac{1}{2}} &= {}^{h}v_{i,j-\frac{1}{2}} - \frac{\delta t}{\delta y}\,\delta\phi_{i,j}
\end{aligned} \tag{10}$$

Here, the superscripts denote the iteration level. This is done for each cell in the mesh. These updated velocities are inserted into Eqn. (7) and the process is repeated until

$$\left| D_{i,j}^{n+1} \right| < \varepsilon \tag{11}$$

for all cells. Here ε is the criterion for iteration convergence. It is noted, however, in this process the iteration error is not cumulative from time step to time step because the residual error from the previous time level is used as a source in the new time level.

During the iteration, just as with the tilde values, no modifications are made to velocities exterior to the computing region or to those values that are located on inflow or rigid boundaries. Hence, this algorithm does not require knowledge of the pressures in fictitious cells outside the computing region.

B. Boundary Conditions

Fictitious computing cells are convenient in applying velocity boundary conditions for use in the convection and viscous stress terms in the momentum equations. At planes of symmetry and rigid walls, the tangential velocity is either continuous with a vanishing gradient in the case of a free-slip boundary or reflective with a zero value at the boundary for the no-slip condition.

A further complication for the calculations is the case of rigid walls that cross the cells diagonally. In Fig. 2 are summarized the four sets of conditions that are required, depending on the spatial location within a cell of the terms in the difference expression and the type of boundary being studied. The velocity components within the rigid wall are specified as indicated in the figure. This treatment has proven successful in recent studies of waves running upon sloping beaches [Amsden (1973)]. A further discussion of velocity conditions for boundaries that cross cell boundaries arbitrarily is found in a recent paper by Viecelli (1971).

A special algorithm has proven quite successful for the boundary condition at continuative outflow boundaries. The tangential component of velocity is assumed continuous with no special treatment required for it. For the normal component located on the outflow boundary, a change is made prior to the iteration phase of the calculation. The normal velocity gradient is made to vanish using the tilde value of the normal component velocity one cell upstream of the boundary. Thus, no tilde velocity calculation is needed on the boundary. The iteration procedure then proceeds in the usual manner and modifies all the velocity components in the cell adjacent to the outflow boundary, assuring that the continuity equation is satisfied.

Nichols and Hirt (1971) recently reported on refinements in the treatment of the MAC free surface boundary conditions. In this approach, the use of special marker particles, which follow the free surface, more accurately defines the surface position than had previously been done. These particles are used in addition or in place of the usual Lagrangian marker particles from which the method derives its name. The schematic diagram in Fig. 3 shows the surface markers within the computing region; the shaded region below the surface represents the fluid. Fictitious cells are used in this algorithm and the subscripts, S and F, refer to surface and full cells, respectively. The use of the markers permits the application of the normal and tangential stress conditions at the actual fluid surface. The pressure in the surface cell is specified as a linear interpolation between the full cell pressure and the pressure that obtains at the free surface as a result of the surface stresses. The distance d in the figure is used in the interpolation procedure and measures the length from the free surface to the center of the full cell.

PARTIAL CELL VELOCITY CONFIGURATIONS

DIFFERENCE EXPRESSIONS

$\frac{\partial v}{\partial x}, \frac{\partial u}{\partial y}, \frac{\partial uv}{\partial x}, \frac{\partial uv}{\partial y}$

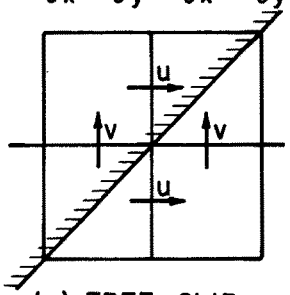

(a) FREE-SLIP

DIFFERENCE EXPRESSIONS

$\frac{\partial u}{\partial x}, \frac{\partial v}{\partial y}, \frac{\partial u^2}{\partial x}, \frac{\partial v^2}{\partial y}$

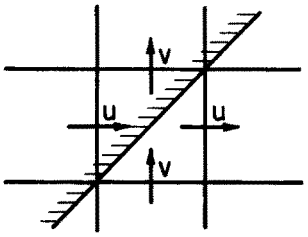

(b) FREE-SLIP

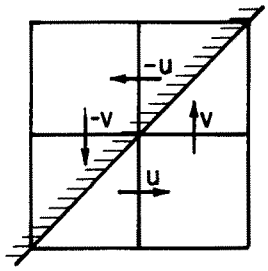

(c) NO-SLIP

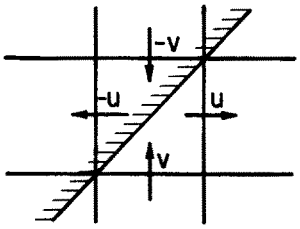

(d) NO-SLIP

los alamos scientific laboratory

Figure 2

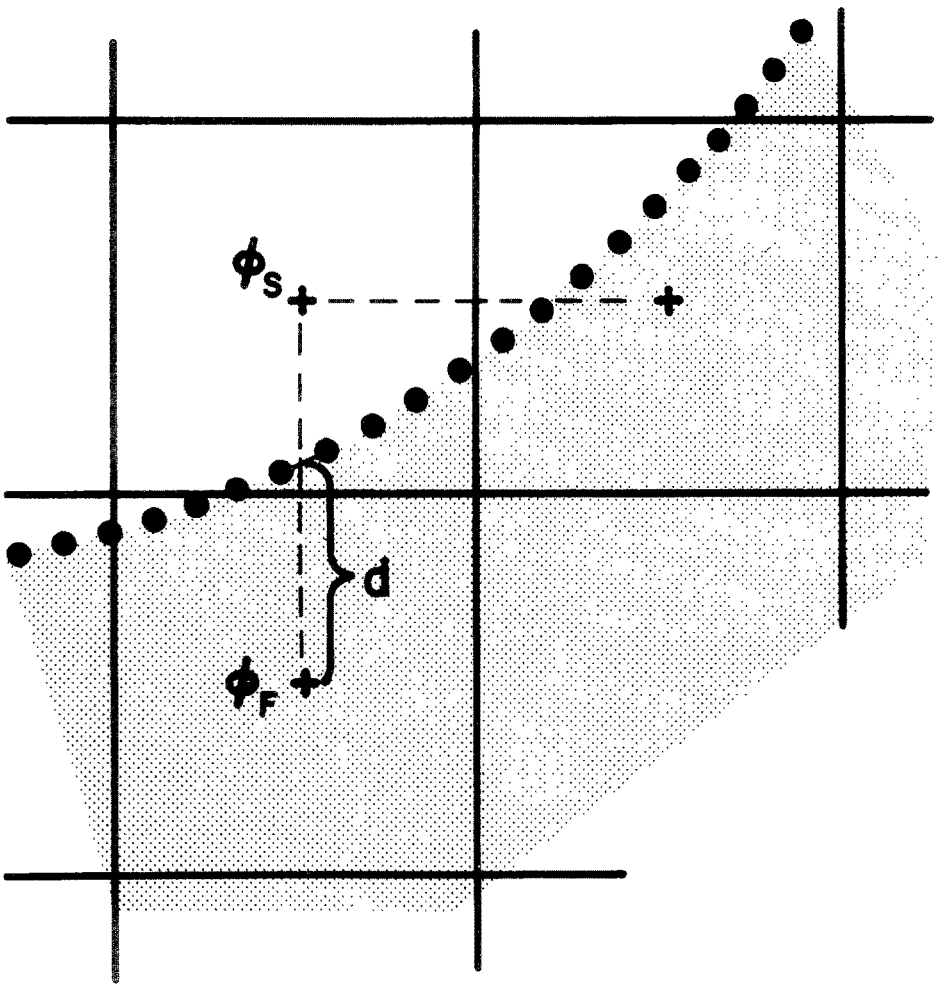

Figure 3

Figure 4 illustrates the effectiveness of this procedure by showing the fluid configuration with and without the surface markers for the problem of a fluid sloshing in a rectangular tank. A cosine-wave pressure pulse at initial time sets the fluid into oscillation. After repeated oscillations the upper frame shows ripples appearing on the free surface; these are not present in the lower frame which uses the surface markers. The ripples result from cell to cell variations in the pressure that cause fictitious accelerations to particles near the surface.

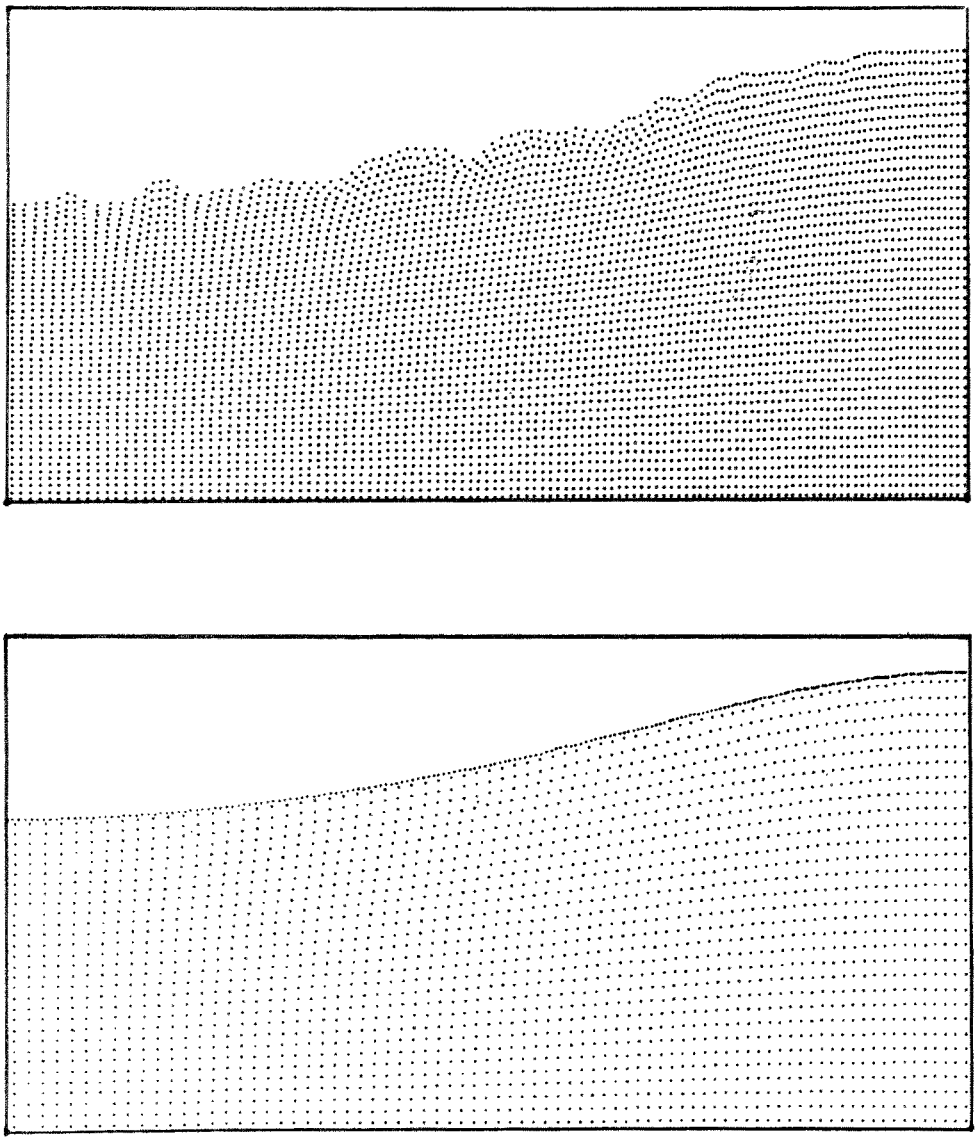

Figure 4

III. THE IMPLICIT CONTINUOUS-FLUID EULERIAN METHOD

The ICE method [Harlow and Amsden (1971)] has been developed to numerically solve multi-dimensional, transient fluid flows of arbitrary Mach number. The implicit formulation of the solution procedure broadens its applicability to flows ranging from supersonic or compressible to far subsonic or incompressible flows. In the incompressible limit, the technique reduces to the MAC method described previously.

The ICE solution procedure implicitly solves the mass and momentum equations and uses an explicit calculation for the energy equation. Harlow and Amsden (1971) determined the pressure field for the momentum equations by the solution of a Poisson equation. Here, however, we present a different method, which is a generalization of the iteration procedure described in the previous section. The advantage of such an approach is the ease of incorporating boundary conditions into the calculations, just as in the case of MAC.

Included in this discussion of the ICE method are two other recent developments. Space does not permit detailed discussion of these and only brief outlines of the developments are presented here. The first is the extension by Butler, et al.,(1973) to permit the application of ICE to multi-component, chemically reacting flows with mixing. The second is a recent investigation by Rivard, et al., (1973) to apply a truncation error canceling scheme to the difference equations used by Butler, et al. This latter technique improves the stability and accuracy of the computing method by locally sensing the diffusional truncation errors inherent in the difference approximation and minimizing their effect on the calculations. Numerical examples showing the effectiveness of this technique are presented.

A. Equations of Motion

The mass and momentum equations for transient flows in two space dimensions for rectangular coordinates are

$$\frac{\partial \rho}{\partial t} + \frac{\partial \rho u}{\partial x} + \frac{\partial \rho v}{\partial y} = 0 \tag{12}$$

$$\frac{\partial \rho u}{\partial t} + \frac{\partial \rho u^2}{\partial x} + \frac{\partial \rho uv}{\partial y} = -\frac{\partial p}{\partial x} + \frac{\partial \sigma_{xx}}{\partial x} + \frac{\partial \sigma_{xy}}{\partial y} \tag{13}$$

$$\frac{\partial \rho v}{\partial t} + \frac{\partial \rho uv}{\partial x} + \frac{\partial \rho v^2}{\partial y} = -\frac{\partial p}{\partial y} + \frac{\partial \sigma_{xy}}{\partial x} + \frac{\partial \sigma_{yy}}{\partial y} \quad , \tag{14}$$

where ρ is the mass density, p is the pressure and the stress tensor components are given by

$$\sigma_{xx} = 2\mu \frac{\partial u}{\partial x} + \lambda \left(\frac{\partial u}{\partial x} + \frac{\partial v}{\partial y} \right)$$

$$\sigma_{xy} = \mu \left(\frac{\partial u}{\partial y} + \frac{\partial v}{\partial x} \right) \qquad (15)$$

$$\sigma_{yy} = 2\mu \frac{\partial v}{\partial y} + \lambda \left(\frac{\partial u}{\partial x} + \frac{\partial v}{\partial y} \right) \quad .$$

In these latter expressions μ and λ are the first and second coefficients of viscosity, respectively.

Equations (12) - (14) are coupled to an equation for the internal energy, ρI:

$$\frac{\partial \rho I}{\partial t} + \frac{\partial \rho I u}{\partial x} + \frac{\partial \rho I v}{\partial y} = (\sigma_{xx} - p) \frac{\partial u}{\partial x} + (\sigma_{yy} - p) \frac{\partial v}{\partial y} + \sigma_{xy} \left(\frac{\partial u}{\partial y} + \frac{\partial v}{\partial x} \right)$$

$$+ \frac{\partial}{\partial x} \left(k \frac{\partial I}{\partial x} \right) + \frac{\partial}{\partial y} \left(k \frac{\partial I}{\partial y} \right) + \dot{q}_c + \dot{q}_D \quad , \qquad (16)$$

where k is the heat conduction coefficient, and $\dot{q}_c$ and $\dot{q}_D$ are source terms to the internal energy representing chemical reactions and enthalpy diffusion resulting from multicomponent species diffusion, respectively.

These are solved together with an equation of state, in which pressure is expressed as a function of ρ and I. For a polytropic gas,

$$p = (\gamma - 1)\, \rho I \qquad (17)$$

where γ is the ratio of specific heats.

To enable the calculation of multi-component species in the flow field, transport equations for the species are written which include convection, diffusion, and creation or decay by chemical reactions:

$$\frac{\partial \rho_\alpha}{\partial t} + \frac{\partial \rho_\alpha u}{\partial x} + \frac{\partial \rho_\alpha v}{\partial y} = \frac{\partial}{\partial x} \left[\rho \eta_\alpha \frac{\partial (\rho_\alpha / \rho)}{\partial x} \right] + \frac{\partial}{\partial y} \left[\rho \eta_\alpha \frac{\partial (\rho_\alpha / \rho)}{\partial y} \right] + (\dot{\rho}_\alpha)_c \quad . \qquad (18)$$

In this equation, the subscript α refers to the species, η_α is an effective binary diffusion coefficient for species α into the multicomponent mixture, and $(\dot{\rho}_\alpha)_c$ represents the source term from chemical reactions. The exact expression for this is discussed by Butler, et al., (1973). This equation is solved subject to the constraints that

$$\sum_{\alpha=1}^{N} \rho_\alpha = \rho \qquad (19)$$

and

$$\sum_{\alpha=1}^{N} \left\{ \frac{\partial}{\partial x} \left[\rho \eta_\alpha \frac{\partial (\rho_\alpha/\rho)}{\partial x} \right] + \frac{\partial}{\partial y} \left[\rho \eta_\alpha \frac{\partial (\rho_\alpha/\rho)}{\partial y} \right] \right\} = 0 \ , \tag{20}$$

where N is the total number of species.

B. Solution Procedure

The finite difference approximations to these equations are similar to those in the previous section. The momentum components ρu and ρv are located on cell boundaries, just as in the MAC case for u and v. Cell centered quantities are ρ, p, and I, together with the variable coefficients μ, λ, and k. The stress tensor components are located at the positions indicated in Fig. 1.

For the total mass density equation, we write

$$\rho^{n+1}_{i,j} = \tilde{\rho}_{i,j} + \theta\, \delta t \left\{ \frac{1}{\delta x} \left[(\rho u)^{n+1}_{i-\frac{1}{2},j} - (\rho u)^{n+1}_{i+\frac{1}{2},j} \right] + \frac{1}{\delta y} \left[(\rho v)^{n+1}_{i,j-\frac{1}{2}} - (\rho v)^{n+1}_{i,j+\frac{1}{2}} \right] \right\} \tag{21}$$

in which $\tilde{\rho}_{i,j}$ is determined from quantities at time level n:

$$\begin{aligned} \tilde{\rho}_{i,j} = \rho^n_{i,j} + \delta t \Bigg\{ & (1-\theta) \left\{ \frac{1}{\delta x} \left[(\rho u)^n_{i-\frac{1}{2},j} - (\rho u)^n_{i+\frac{1}{2},j} \right] + \frac{1}{\delta y} \left[(\rho v)^n_{i,j-\frac{1}{2}} - (\rho v)^n_{i,j+\frac{1}{2}} \right] \right\} \\ & + \frac{1}{\delta x^2} \left[\tau_{i+\frac{1}{2},j} \left(\rho^n_{i+1,j} - \rho^n_{i,j} \right) - \tau_{i-\frac{1}{2},j} \left(\rho^n_{i,j} - \rho^n_{i-1,j} \right) \right] \\ & + \frac{1}{\delta y^2} \left[\tau_{i,j+\frac{1}{2}} \left(\rho^n_{i,j+1} - \rho^n_{i,j} \right) - \tau_{i,j-\frac{1}{2}} \left(\rho^n_{i,j} - \rho^n_{i,j-1} \right) \right] \Bigg\} \ . \end{aligned} \tag{22}$$

In these equations, θ is a parameter used to vary the relative time centering of the convection terms. It ranges in value from zero for a purely explicit calculation to unity for a completely time advanced treatment of the convection terms. The value, θ=.5, is usually chosen for most compressible flow calculations because this choice eliminates first order time errors that arise in the difference approximation.

The diffusion terms in Eqn. (22) are added to assure stability of the numerical calculations and yet minimize the effects of the lowest order truncation errors inherent in the finite difference equations. These errors may result in either excessive numerical diffusion or insufficient diffusion to stabilize the calculations. The form of the necessary diffusion terms was suggested by Hirt (1968) after examining the stability properties of the non-linear equations.

With θ=.5, the expressions for these diffusion coefficients are

$$\tau_{i+\frac{1}{2},j} = (1 + \xi)\,\frac{\delta x}{8}\,\Delta u \qquad \text{if } \Delta u \geq 0$$

or (23)

$$\tau_{i+\frac{1}{2},j} = (1 - \xi)\,\frac{\delta x}{8}\,\Delta u \qquad \text{if } \Delta u < 0 \quad ,$$

where $\Delta u = u^{n}_{i+3/2,j} - u^{n}_{i-\frac{1}{2},j}$.

The value of ξ ranges $0 < \xi < 1$ with many problems requiring $\xi \leq .2$. Analogous expressions to those in Eqn. (23) are used for the other coefficients in Eqn. (22).

This procedure of variable coefficients of diffusion has proven very successful in a wide variety of problems tested. It has obvious advantages over the scheme originally proposed for ICE because it automatically supplies the necessary diffusion for stability and applies it only in regions where needed. The value of ξ is usually held fixed and is greater than zero to allow sufficient smoothing to overcome truncation errors of higher order that were neglected in the error analysis.

Similar expressions to Eqns. (22) and (23) have been derived for each of the ICE difference equations. The report by Rivard, et al., (1973) presents them in detail, and we shall not repeat them here. However, the calculational examples at the end show their effect over using usual artificial viscosity stabilizing methods.

The finite difference approximation to Eqn. (13) is

$$(\rho u)^{n+1}_{i+\frac{1}{2},j} = (\widetilde{\rho u})_{i+\frac{1}{2},j} + \frac{\delta t}{\delta x}\left[\bar{p}_{i,j} - \bar{p}_{i+1,j}\right] \tag{24}$$

where the tilde value is computed from quantities at time level n and the $\bar{p}$ values are found by iteration in satisfying the mass equation. The intermediate momentum component is written

$$(\widetilde{\rho u})_{i+\frac{1}{2},j} = (\rho u)^{n}_{i+\frac{1}{2},j} + \delta t \left\{ \frac{1}{\delta x}\left[p^{n}_{i,j} - p^{n}_{i+1,j} + (\rho u^2)_{i,j} - (\rho u^2)_{i+1,j} \right.\right.$$

$$\left. + (\sigma_{xx})_{i+1,j} - (\sigma_{xx})_{i,j} \right] + \frac{1}{\delta y}\left[(\rho uv)_{i+\frac{1}{2},j-\frac{1}{2}} - (\rho uv)_{i+\frac{1}{2},j+\frac{1}{2}} \right.$$

$$\left.\left. + (\sigma_{xy})_{i+\frac{1}{2},j+\frac{1}{2}} - (\sigma_{xy})_{i+\frac{1}{2},j-\frac{1}{2}} \right] \right\} \tag{25}$$

neglecting the truncation error cancellation terms. The terms on the right hand side are computed using straightforward averages and centered differences of the quantities at time level n. Difference equations similar to Eqns. (24) and (25) are found for $(\rho v)^{n+1}_{i,j+\frac{1}{2}}$ in solving Eqn. (14).

New values of total mass density and momenta for the time step are found in the same way as described in Eqns. (6) - (11). In this case, however, we define

$$D_{i,j} = \rho_{i,j} - \tilde{\rho}_{i,j} + \theta\,\delta t \left\{ \frac{1}{\delta x}\left[(\rho u)_{i+\frac{1}{2},j} - (\rho u)_{i-\frac{1}{2},j}\right] + \frac{1}{\delta y}\left[(\rho v)_{i,j+\frac{1}{2}} - (\rho v)_{i,j-\frac{1}{2}}\right]\right\} \tag{26}$$

and

$$\delta\bar{p}_{i,j} = -\frac{\omega D_{i,j}}{\left(\frac{\partial D}{\partial \bar{p}}\right)_{i,j}} \quad . \tag{27}$$

The denominator is evaluated as

$$\left(\frac{\partial D}{\partial \bar{p}}\right)_{i,j} = \frac{1}{(c^2)_{i,j}} + 2\theta\delta t^2\left(\frac{1}{\delta x^2} + \frac{1}{\delta y^2}\right)$$

in which $(c^2)_{i,j}$ is the square of the sound speed determined from the equation of state using the definition

$$\left(\frac{\partial p}{\partial \rho}\right) = c^2 \quad .$$

Once $\delta\bar{p}_{i,j}$ is determined the quantities are updated as in Eqn. (10):

$$\begin{aligned}
{}^{h+1}\bar{p}_{i,j} &= {}^{h}\bar{p}_{i,j} + \delta\bar{p}_{i,j} \\
{}^{h+1}\rho_{i,j} &= {}^{h}\rho_{i,j} + \frac{\delta\bar{p}_{i,j}}{(c^2)_{i,j}} \\
{}^{h+1}(\rho u)_{i+\frac{1}{2},j} &= {}^{h}(\rho u)_{i+\frac{1}{2},j} + \frac{\delta t}{\delta x}\,\delta\bar{p}_{i,j} \\
{}^{h+1}(\rho u)_{i-\frac{1}{2},j} &= {}^{h}(\rho u)_{i-\frac{1}{2},j} - \frac{\delta t}{\delta x}\,\delta\bar{p}_{i,j} \\
{}^{h+1}(\rho v)_{i,j+\frac{1}{2}} &= {}^{h}(\rho v)_{i,j+\frac{1}{2}} + \frac{\delta t}{\delta y}\,\delta\bar{p}_{i,j} \\
{}^{h+1}(\rho v)_{i,j-\frac{1}{2}} &= {}^{h}(\rho v)_{i,j-\frac{1}{2}} - \frac{\delta t}{\delta y}\,\delta\bar{p}_{i,j}
\end{aligned} \tag{28}$$

The superscripts denote the iteration levels. These updated quantities are substituted into Eqn. (26) and the process is repeated in all computing cells until

$$\left| D_{i,j}^{n+1} \right| < \varepsilon \quad .$$

With the completion of the iteration procedure, new velocities are determined from the momenta and densities:

$$u_{i+\frac{1}{2},j}^{n+1} = \frac{(\rho u)_{i+\frac{1}{2},j}^{n+1}}{.5\left(\rho_{i,j}^{n+1} + \rho_{i+1,j}^{n+1}\right)} \tag{29}$$

$$v_{i,j+\frac{1}{2}}^{n+1} = \frac{(\rho v)_{i,j+\frac{1}{2}}^{n+1}}{.5\left(\rho_{i,j}^{n+1} + \rho_{i,j+1}^{n+1}\right)} \quad .$$

These updated values of velocity and pressure are used in the explicit calculation for the internal energy:

$$\begin{aligned}(\rho I)_{i,j}^{n+1} = (\rho I)_{i,j}^{n} + \delta t \Bigg\{ & \frac{1}{\delta x}\left[(\rho Iu)_{i-\frac{1}{2},j} - (\rho Iu)_{i+\frac{1}{2},j} + (\sigma_{xx} - \overline{p})_{i,j}\left(u_{i+\frac{1}{2},j}^{n+1} - u_{i-\frac{1}{2},j}^{n+1}\right)\right] \\ & + \frac{1}{\delta y}\left[(\rho Iv)_{i,j-\frac{1}{2}} - (\rho Iv)_{i,j+\frac{1}{2}} + (\sigma_{yy} - \overline{p})_{i,j}\left(v_{i,j+\frac{1}{2}}^{n+1} - v_{i,j-\frac{1}{2}}^{n+1}\right)\right] \\ & + (\sigma_{xy})_{i,j}\left[\frac{1}{\delta y}\left(u_{i,j+\frac{1}{2}}^{n+1} - u_{i,j-\frac{1}{2}}^{n+1}\right) + \frac{1}{\delta x}\left(v_{i+\frac{1}{2},j}^{n+1} - v_{i-\frac{1}{2},j}^{n+1}\right)\right] \\ & + \frac{1}{\delta x^2}\left[k_{i+\frac{1}{2},j}\left(I_{i+1,j}^{n} - I_{i,j}^{n}\right) - k_{i-\frac{1}{2},j}\left(I_{i,j}^{n} - I_{i-1,j}^{n}\right)\right] \\ & + \frac{1}{\delta y^2}\left[k_{i,j+\frac{1}{2}}\left(I_{i,j+1}^{n} - I_{i,j}^{n}\right) - k_{i,j-\frac{1}{2}}\left(I_{i,j}^{n} - I_{i,j-1}^{n}\right)\right] \\ & + (\dot{q}_c)_{i,j} + (\dot{q}_D)_{i,j} \Bigg\}\end{aligned} \tag{30}$$

in which the convection terms are formed by straightforward averages of the internal energy at time level n and the new velocities.

Explicit calculations are also made to determine the new species densities. The difference approximation to Eqn. (18) is given by

$$(\rho_\alpha)^{n+1}_{i,j} = (\rho_\alpha)^{n}_{i,j} + \delta t \left\{ \frac{1}{\delta x}\left[(\rho_\alpha u)_{i-\frac{1}{2},j} - (\rho_\alpha u)_{i+\frac{1}{2},j}\right] + \frac{1}{\delta y}\left[(\rho_\alpha v)_{i,j-\frac{1}{2}} - (\rho_\alpha v)_{i,j+\frac{1}{2}}\right] \right.$$

$$+ \frac{1}{\delta x^2}\left\{(\rho\eta_\alpha)_{i+\frac{1}{2},j}\left[(\rho_\alpha/\rho)_{i+1,j} - (\rho_\alpha/\rho)_{i,j}\right]\right.$$

$$\left. - (\rho\eta_\alpha)_{i-\frac{1}{2},j}\left[(\rho_\alpha/\rho)_{i,j} - (\rho_\alpha/\rho)_{i-1,j}\right]\right\}$$

$$+ \frac{1}{\delta y^2}\left\{(\rho\eta_\alpha)_{i,j+\frac{1}{2}}\left[(\rho_\alpha/\rho)_{i,j+1} - (\rho_\alpha/\rho)_{i,j}\right]\right.$$

$$\left. - (\rho\eta_\alpha)_{i,j-\frac{1}{2}}\left[(\rho_\alpha/\rho)_{i,j} - (\rho_\alpha/\rho)_{i,j-1}\right]\right.$$

$$\left. + \left[(\dot{\rho}_\alpha)_c\right]_{i,j}\right\} \quad . \tag{31}$$

The convection terms again are formed using species densities at time level n and the new velocities. In order to ensure strict mass conservation, N-1 species transport equations are solved with the N^{th} species determined using Eqn. (19):

$$(\rho_N)^{n+1}_{i,j} = \rho^{n+1}_{i,j} - \sum_{\alpha=1}^{N-1} (\rho_\alpha)^{n+1}_{i,j} \quad . \tag{32}$$

A special algorithm has been developed to impose the constraint of Eqn. (20). The essence of the algorithm is to simultaneously consider the diffusion terms for each species in Eqn. (31) and ensure that no net mass transport is accomplished during the time step by the diffusional process. This is achieved by monitoring the diffusional fluxes across each boundary of the computing cell and limiting the amount of diffusion such that Eqn. (20) is satisfied.

C. Example Calculations

An often used treatment to assure numerical stability of the calculations is to use fictitiously large values of the viscosity coefficients, μ and λ, to overcome the effects of truncation errors resulting from the difference approximations. Harlow and Amsden (1971) state the choices for μ and λ in such an approach are given by:

$$\mu, \lambda \gtrsim 3/2\ \rho\ u^2_{max}\ \delta t + \rho_{max}\left(\frac{\partial u}{\partial x}\right)_{max} \delta x^2 \tag{33}$$

where the subscripts refer to the maximum values for the velocity, density and velocity gradients in the computing mesh. This choice, while ensuring numerical stability, may produce large inaccuracies in the calculational results because of excessive numerical diffusion. This is especially true when the flow is directed primarily in one coordinate direction, such as in the case of flow down a uniform channel.

Consider the flow configuration shown schematically in Fig. 5. A perfect gas, with specific heat ratio $\gamma = 1.4$, enters on the left with a velocity profile symmetric about the centerline of the channel. The horizontal velocity grades linearly from a magnitude $u = 1.0$ at the adiabatic, free-slip channel walls to $u = 0.2$ at the centerline. The flow is everywhere supersonic with a uniform temperature across the channel, and the flow Mach number based on the velocity at the walls is $M = 10.0$. The right boundary of the computing region is a continuative outflow boundary. With this configuration for an inviscid fluid, the exact solution of this idealized problem has no x-dependence at steady state with the inflow velocity profile reproduced at any axial location downstream of the inflow boundary.

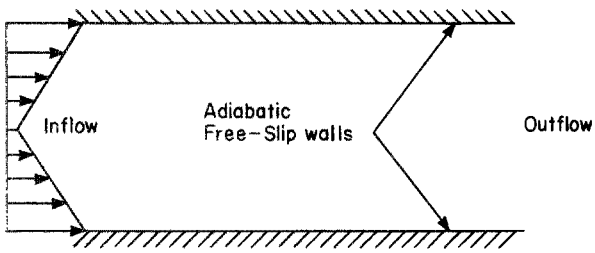

Figure 5

The results of two different calculations of this problem are summarized in Fig. 6.

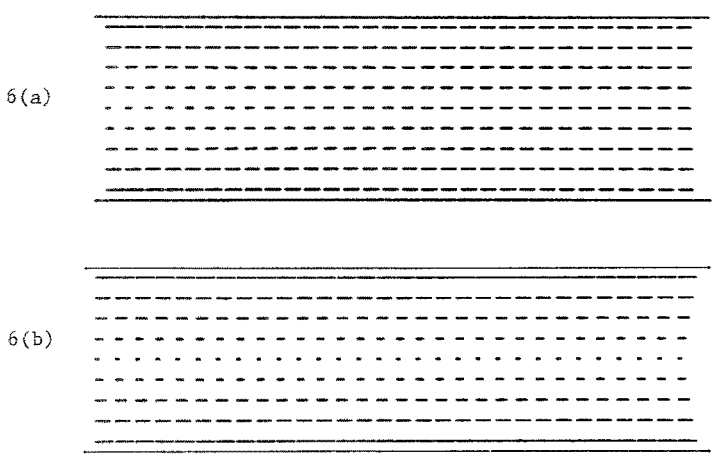

Figure 6

Both calculations started with identical initial conditions of a uniform velocity u = 1.0 in all cells except those at the left boundary. These are plots of the velocity vectors in each cell after the flow has achieved steady state. Fig. 6(a) shows the velocities computed using the criteria for μ and λ given in Eqn. (33), which are essentially the minimum values for stability. In this case, the centerline velocity is accelerated down the length of the channel and the wall velocities drop in magnitude until an almost uniform velocity profile is produced at the outflow boundary, a consequence of the fictitious viscosity acting in the transverse direction.

The calculation shown in Fig. 6(b) is that using the truncation error cancellation method of Rivard, et al., (1973) to achieve stability. Excellent agreement is noted in this case with the velocity field at each axial location corresponding to the inflow profile to within less than 0.2% error.

As a more comprehensive example problem, we consider the flow in a continuous wave chemical laser. The flow configuration is that shown schematically in Fig. 7.

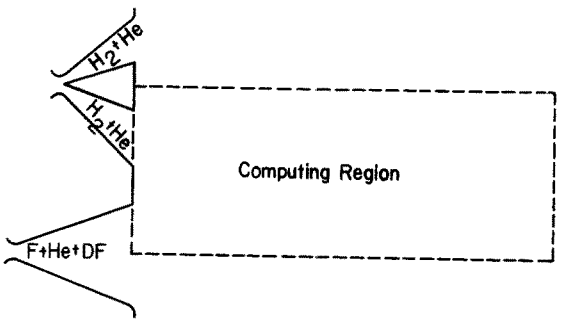

Figure 7

A series of two-dimensional slit nozzles flowing a mixture of F, He, and DF are alternately interspersed with split nozzles admitting H_2 and He. Downstream of each pair of nozzles, the H_2 and F mix and react exothermically to produce vibrationally excited HF molecules, which serve as the lasing medium. The computing mesh extends from the nozzle exit plane downstream to a continuative outflow boundary with symmetry boundaries at the top and bottom. The vertical span for the mesh extends from the centerline of the hydrogen stream to the centerline of the fluorine stream. The Mach number of the flow exiting the lower nozzle is M = 3.5 and for the upper nozzle, M = 3.7.

Figure 8(a) shows the steady state velocity vectors from the calculations using μ and λ obtained from Eqn. (33), and Fig. 8(b) shows the results using the truncation error cancellation method.

8(a)

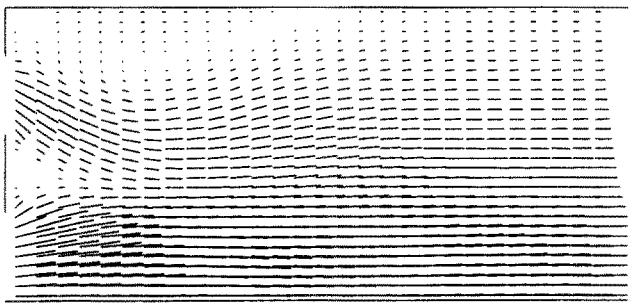

8(b)

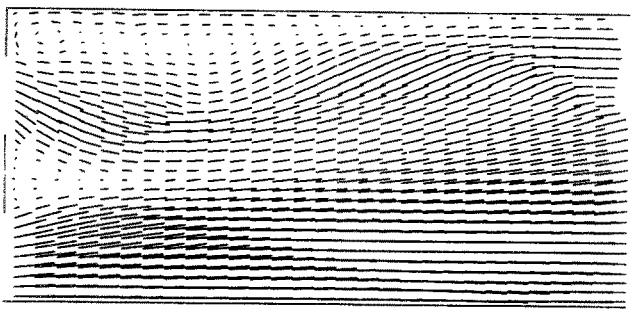

Figure 8

In (a), the inflow velocity profiles are rapidly smoothed downstream because of the excessive kinetic energy dissipation brought about by the artificially high values of viscosity necessary for stability. Such is not the case in (b). In addition, the recirculation region in the upper left corner of the mesh is much more pronounced in (b) and a shock caused by the collision of the H_2 stream with the upper symmetry boundary is seen in (b) but is not present in (a) because of the large kinetic energy dissipation.

IV. REFERENCES

Amsden, A. A., "Numerical Calculation of Surface Waves: A Modified ZUNI Code with Surface Particles and Partial Cells," Los Alamos Scientific Laboratory Report LA-5146 (1973).

Butler, T. D., Farmer, O. A., and Rivard, W. C., "A Numerical Technique for Transient, Chemically Reactive Flows of Arbitrary Mach Number," Los Alamos Scientific Laboratory Report to be published (1973).

Harlow, F. H. and Welch, J. E., Phys. Fluids 8, 2182 (1965).

Harlow, F. H., "Numerical Methods for Fluid Dynamics - An Annotated Bibliography," Los Alamos Scientific Laboratory Report LA-4281 (1969).

Harlow, F. H., and Amsden, A. A., J. Comp. Phys. 6, 322 (1970).

Harlow, F. H., and Amsden, A. A., J. Comp. Phys. 8, 197 (1971).

Hirt, C. W., J. Comp. Phys. 2, 339 (1968).

Hirt, C. W. and Cook, J. L., J. Comp. Phys. 10, 324 (1972).

Nichols, B. D. and Hirt, C. W., J. Comp. Phys. 8, 434 (1971).

Rivard, W. C., Butler, T. D., Farmer, O. A., and O'Rourke, P. J., "A Method for Increased Accuracy in Eulerian Fluid Dynamics Calculations," Los Alamos Scientific Laboratory Report LA-5426-MS (1973).

Viecelli, J. A., J. Comp. Phys. 8, 119 (1971).